Proceedings of The Institute of Acoustics

New Transducer Concepts at the Naval Research Laboratory

A.L. Van Buren, P.H. Rogers, J.F. Zalesak and R.L. Phillips

Underwater Sound Reference Division, Naval Research Laboratory, Orlando, Florida, U.S.A.

Introduction

We describe four new sonar transducer concepts being developed at the Naval Research Laboratory. The first two concepts are directional hydrophones. One is a low-frequency directional ring hydrophone that provides a $\cos^2\theta$ quadrupole farfield pattern over a wide band of low frequencies. The other is a dielectric liquid hydrophone that provides a quadrupole-like farfield pattern together with a flat receiving voltage sensitivity over a wide frequency band. The third concept is a critical-angle fiber-optic hydrophone that is based on a very short section of optical fiber. The fourth concept is a constant beamwidth transducer that provides frequency-independent low-sidelobe farfield patterns over a wide frequency band and is usable both as a projector and a receiver.

I. Low-Frequency Directional Ring Hydrophone

In its simplest form the low-frequency directional ring hydrophone [1] is a free-flooded piezoceramic tube or ring, as shown in Fig. 1. The receiving farfield pattern of a free-flooded ring at low frequencies is composed of two components. The first component is an omnidirectional monopole that is independent of frequency. The second component is a $\sin^2\theta$ or doughnut-shaped quadrupole that varies as the square of the frequency. When the ring is circumferentially polarized, these two components are of opposite sign. They combine at some low frequency to give a $\cos^2\theta$ pattern. The $\cos^2\theta$ pattern (or nearly so) is maintained over a frequency band about one-half an octave wide. Compared to the cos pattern of a dipole, the $\cos^2\theta$ pattern is narrower and has more directivity. In addition, its top-bottom symmetry makes the low-frequency directional ring hydrophone insensitive to acceleration, while the dipole is essentially an accelerometer.

We can greatly increase the bandwidth of the low-frequency directional ring hydrophone by use of an alternate, although less simple, design. In this design, as seen in Fig. 2, the free-flooded ring is combined with an omnidirec-

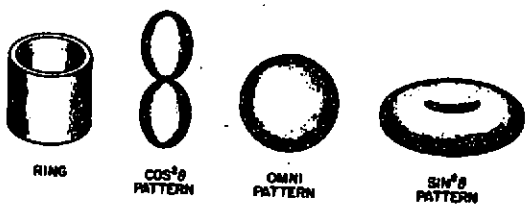

Fig. 1. Free-flooded ring with pattern components.

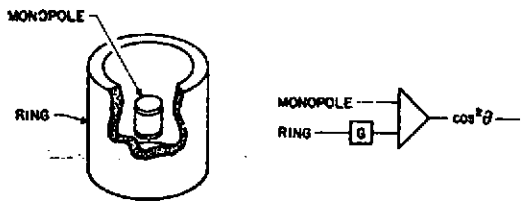

Fig. 2. Ring-monopole combination.

tional monopole. The signal received by the ring is added, with appropriate weighting, to that of the monopole to produce the $\cos^2\theta$ pattern. The ring can be circumferentially, radially, or height polarized. We allow the weighting factor G to be frequency dependent so that the device can operate over a broad frequency range.

We investigated a ring-monopole combination in which the ring is radially polarized. The piezoceramic ring is 25 mm high, 25 mm in diameter, and 1.5 mm thick. The monopole at the center of the ring is a small capped piezoceramic tube that is also radially polarized. The weighting factor was adjusted to produce a receiving pattern as close as possible to $\cos^2\theta$. Good patterns were obtained over a frequency band extending from 2.5 to 30 kHz. Typical of the results is the pattern shown in Fig. 3 for 10 kHz. The dashed line is the ideal $\cos^2\theta$ pattern.

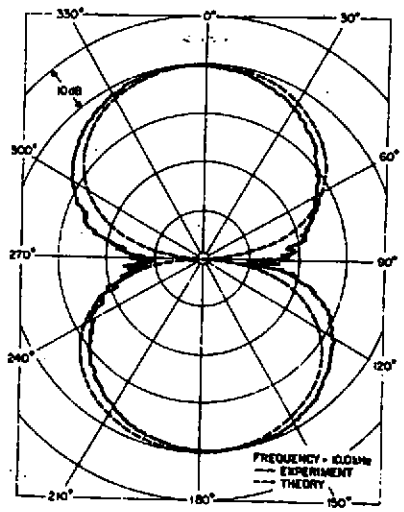

Fig. 3. Farfield pattern of ring-monopole combination at 10 kHz.

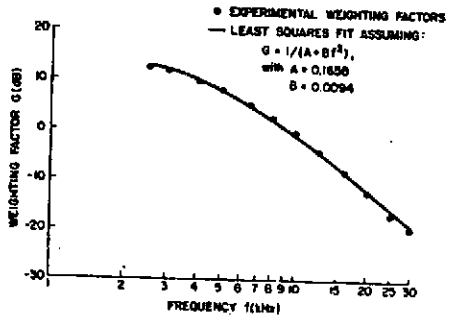

Fig. 4. Weighting factors for ring-monopole combination.

The values for the weighting factor G as determined experimentally to produce the best $\cos^2\theta$ pattern are plotted in Fig. 4 as a function of frequency. They are represented by circles and plotted in decibels. The solid curve is a least-squares fit to the experimental data assuming the simple frequency dependence for G given in the figure legend. We constructed an analog shading box to provide weighting factors according to the solid curve of Fig. 4. Experimentally measured patterns using the shading box were similar to those obtained earlier, although the nulls were not as deep. The shallower nulls were probably due to non-zero phase angles appearing in the weighting factors produced by the shading box.

If three low-frequency directional ring hydrophones are oriented in a plane at 120° with respect to each other, then a $\cos^2\theta$ pattern can be steered anywhere within the plane by using electronic circuitry just slightly more complex than that used to steer dipoles. If two low-frequency directional ring hydrophones are oriented at some angle with respect to each other and placed in a sound field, then their relative outputs can be used to determine the bearing of the source of sound just as it is done using dipole transducers.

II. Dielectric Liquid Hydrophone

The dielectric liquid hydrophone is envisioned to be a pillbox-shaped device, as seen in Fig. 5. It has thin rubbery walls, is filled with a dielectric liquid, and has flexible electrodes on both the top and bottom surfaces. A large d.c. bias voltage is applied across the electrodes. The dielectric liquid is chosen to have a sound speed c and density ρ similar to water, and the rubbery walls are chosen to be highly transparent to sound. An incoming sound wave thus passes unchanged through the hydrophone. As it passes, however, it modulates the bias voltage by changing both the dimensions and dielectric constant ϵ of the hydrophone. The sound wave is detected by monitoring this voltage modulation.

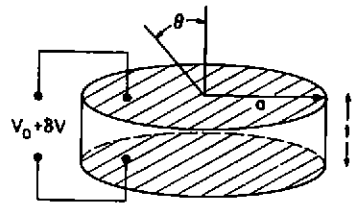

$$M = \frac{\delta V}{p} = -\frac{V_0}{\rho c^2}\left[2\cos^2\theta - \frac{a}{t}\,|\sin\theta\cos\theta| - (1-\rho c^2\frac{\partial\epsilon}{\partial p})\right]$$

Fig. 5. Dielectric liquid hydrophone.

We obtain by elementary calculations the low frequency approximation for the receiving voltage sensitivity M that is given in Fig. 5. If the dimensions are chosen so that a>>t, then the receiving farfield pattern consists of a quadrupole-like $\cos^2\theta$ term together with a monopole term $\rho c^2 \partial\varepsilon/\partial p - 1$. We note that the receiving voltage sensitivity is independent of frequency. By selecting the dielectric liquid carefully, we may be able to obtain farfield patterns that vary from a quadrupole of the form $2\cos^2\theta - 1 = \cos 2\theta$ (when $\rho c^2 \partial\varepsilon/\partial p \ll 1$) to a monopole (when $\rho c^2 \partial\varepsilon/\partial p \gg 1$) to a $\cos^2\theta$ quadrupole similar to that of the low-frequency directional ring hydrophone (when $\rho c^2 \partial\varepsilon/\partial p = 1$).

We plan to experimentally test this concept in the near future. We will also test an alternative design using RHO-C rubber in place of the liquid and rubbery walls. The ends of the rubber cylinder can be carbon impregnated to provide the flexible electrodes.

III. Critical-Angle Fiber-Optic Hydrophone

Previous fiber-optic hydrophone concepts [1] are based on an integrated effect over moderately long lengths of optical fiber. We describe in this paper an alternative concept that requires only a short section of optical fiber, as seen in Fig. 6. The end face of the fiber is polished to an angle near the critical angle appropriate for a glass fiber water interface. When an optical wave produced by a laser propagates down the fiber core and is incident on the glass-water interface, part of its energy is reflected into the fiber jacket where it is reflected from the flattened mirrored surface. It is then coupled back into the fiber core to produce a returned wave. Both the amplitude and the phase of the returned wave depend on the relative index of refraction for glass and water. This dependence is very strong in the region of the critical angle. In this region small perturbations in the relative index of refraction due to an incident sound wave can produce large variations in the amplitude or phase of the returned optical wave. The sound wave can then be detected by monitoring these variations.

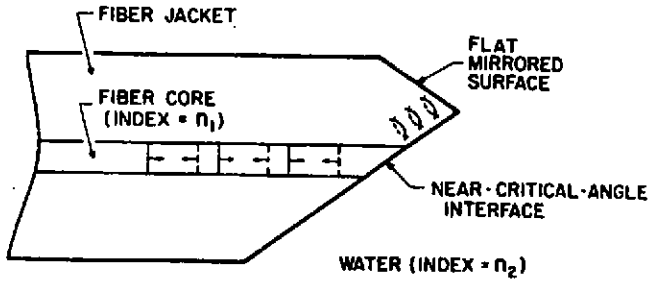

Fig. 6. Critical-angle fiber-optic hydrophone.

The relection of a plane optical wave from a planar interface between two dielectrics is described by the well-known Fresnel equations. These equations show that the amplitude of the reflected wave changes very rapidly with respect to the relative index of refraction when the angle of incidence is slightly less than the critical angle. Similarly, the phase of the reflected wave changes rapidly with respect to the relative index of refraction when the angle of incidence is slightly greater than the critical angle. We see this behavior in Figs. 7 and 8 for the case where the optical wave is plane-polarized parallel to the plane of incidence. Here we have plotted, as a function of the angle of incidence, the rate of change of both the reflectivity R and the phase angle ϕ with respect to the relative index of refraction n. The value for n was chosen to be representative of a glass-water interface. The corresponding behavior when the optical wave is plane-polarized perpendicular to the plane of incidence is very similar to that shown here.

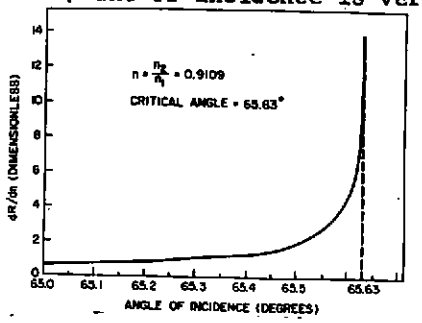

Fig. 7. Plot of dR/dn versus angle of incidence.

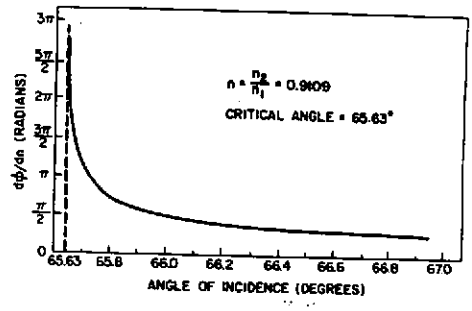

Fig. 8. Plot of dφ/dn versus angle of incidence.

The curves of Figs. 7 and 8 are appropriate for plane waves. We will use a single-mode fiber to restrict the optical wave propagating in the fiber to the fundamental or plane-wave mode. Although the complicated wave behavior at the glass-water interface is probably not identical to that of plane waves, the Fresnel equations should at least qualitatively describe the reflection physics. Thus we expect the optical wave returned from the interface to be amplitude or phase modulated when an incoming sound wave modulates the relative index of refraction. The returned optical wave can be directly detected if the wave has been amplitude modulated or it can be homodyne detected if it has been phase modulated. For homodyne detection the first surface reflection from the input end of the fiber can be used as the reference wave. This would make the homodyne detection self-aligning.

The degree of modulation of the optical wave depends on the degree to which the relative index of refraction changes with pressure. Calculations show that for glass and water and for light in the visible band, $\Delta n \sim 10^{-10} \Delta p$, where the acoustic pressure Δp is in Pa. The small factor 10^{-10} requires

that the end of the optical fiber be polished at an angle that is within about 0.01^{o} from the critical angle in order to detect small sound pressures. Since the critical angle depends on the ambient temperature and pressure, we must be able to retune the system when they change. One way to do this is to vary the wavelength of the optical wave by use of a tunable laser. The relative index of refraction of glass and water and hence the critical angle depends strongly on the optical wavelength.

The analysis given above suggests that sound can be detected using a short length of optical fiber whose end is polished near the critical angle. A fiber optic hydrophone based on this concept is presented being fabricated, and test results will be available shortly.

IV. Constant Beamwidth Transducer

Most directional transducers and arrays exhibit beam patterns which are frequency dependent. Thus, the spectral content of the transmitted or received signal varies with position in the beam and the fidelity of an underwater acoustic system depends on the relative orientation of the transmitter and receiver. We describe here a simple method for obtaining a transducer whose beamwidth is essentially independent of frequency over a broad bandwidth. Our constant beamwidth transducer (CBT) [4,5], as shown in Fig. 9, is a rigid spherical cap of arbitrary half angle α_ν shaded so that the normal velocity on the outer surface is proportional to $P_\nu(\cos\theta)$, where P_ν is the Legendre function whose root of smallest angle occurs at $\theta=\alpha_\nu$.

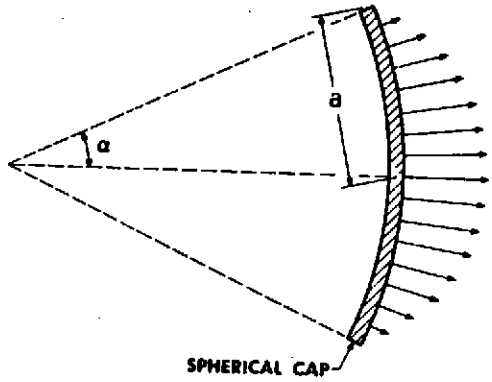

Fig. 9. Constant beamwidth transducer.

Theoretical calculations show that the CBT has uniform acoustic loading, extremely low sidelobes, and an essentially constant beam pattern for all frequencies above a certain cutoff frequency.

The key to the special properties of the CBT is its Legendre function velocity distribution. We show in Fig. 10 the velocity distributions for

a P_5 CBT, $P_{7.5}$ CBT, and P_{10} CBT. The order ν of the Legendre function can be chosen to be any real number greater than zero. The corresponding angle decreases monotonically from near 180° as α_ν increases from just above zero. We present in Fig. 11 a graph of α_ν as a function of ν. Included is a graph of the -3 dB half angle y_ν. Also included in the figure legends are excellent approximations describing the curves. Reference 5 provides additional formulas useful in the design of a CBT. The formulas involve simple algebraic and trigonometric expressions and are readily evaluated using a pocket calculator.

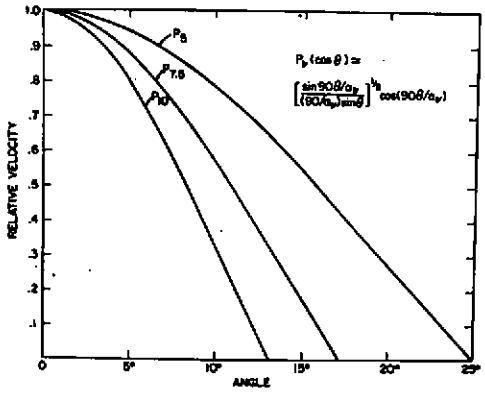

Fig. 10. Velocity distributions for a P_5 CBT, $P_{7.5}$ CBT, and P_{10} CBT.

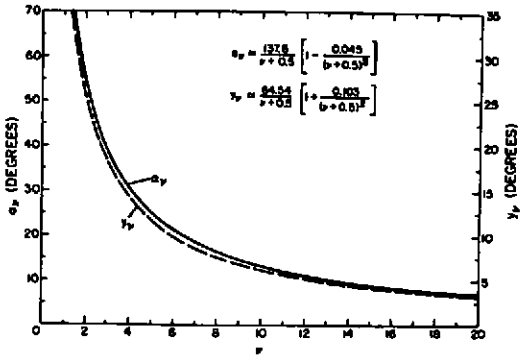

Fig. 11. Cap half angle and -3 dB angle versus the order ν of the Legendre function.

The beam pattern of the CBT resembles the normal velocity distribution at high frequencies. As the frequency decreases from high to low values, the patterns tend to resemble the high frequency limit less and less. The highest frequency below which the resemblance is less than acceptable is called the low-frequency cutoff f_c. A general rule of thumb for the cutoff frequency in kHz is given by $f_c = [1.10 + (24.6/y_\nu)]/b$, where b is the half arclength (i.e., radius) of the spherical cap in meters and y_ν is in degrees. Figure 12 shows the calculated range of beam patterns for a $P_{7.5}$ CBT, both for frequencies above the cutoff frequency f_c (indicated by the total shaded region) and for frequencies above 2 f_c (indicated by the dark shaded region). We note the virtual absence of sidelobes.

The transmitting current response of the CBT under piezoelectric drive is nearly constant for a wide band of frequencies above the cutoff frequency. We see this behavior in Fig. 13 for a P_5 CBT. The transmitting current response for both a circular piston and a uniformly shaded cap are shown for comparison.

We envision the CBT as being a mosaic of small piezoelectric ceramic elements mounted on a backing plate in the shape of a spherical cap. If the operating depth is no greater than about 300 m, corprene or other pressure-

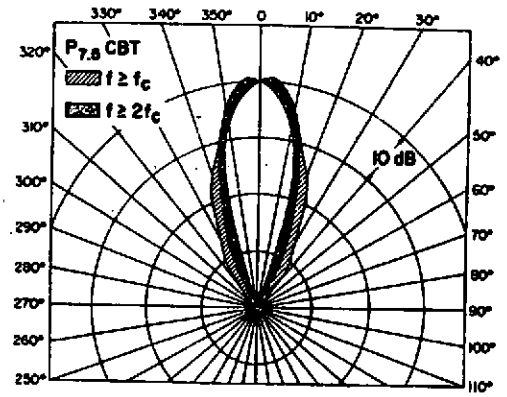

Fig. 12. Range of beam patterns for a $P_{7.5}$ CBT.

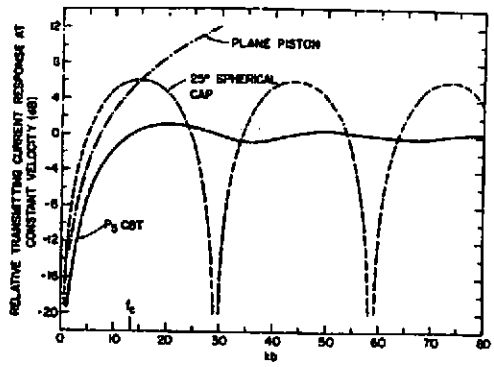

Fig. 13. Transmitting current response for a P_5 CBT, a plane piston, and a 25° uniformly shaded cap.

release material can be used to isolate the elements from each other and from the backing plate. The elements should be arranged on the cap in circular bands with constant θ boundaries. We can then stepwise approximate the continuous velocity distribution by driving each band of elements in relation to the average value of P_ν over the band. Numerical calculations show that subdivision into 10 or more bands of approximately equal angular widths results in excellent constant beamwidth behavior. The surface need not be entirely covered with ceramic. For example, circular ceramic pieces can be used, if desired.

Our constant beamwidth transducer concept is equally applicable to receivers. We are presenting constructing a P_5 CBT to be used both as a projector and a receiver.

References

1. J. F. Zalesak and P. H. Rogers, "Low-frequency radiation characteristics of free-flooded ring transducers with application to a low-frequency directional hydrophone," J. Acoust. Soc. Am. 56, 1052 (1974).
2. J. A. Bucaro, H. D. Dardy, and E. F. Carome, "Fiber-optic hydrophone," J. Acoust. Soc. Am. 62, 1302 (1977).
3. R. L. Phillips, "Proposed fiber-optic acoustical probe," Opt. Lett. 5, 318 (1980).
4. P. H. Rogers and A. L. Van Buren, "New approach to a constant beamwidth transducer," J. Acoust. Soc. Am. 64, 38 (1978).
5. A. L. Van Buren, "Design manual for a constant beamwidth transducer," NRL Rpt. No. 8329 (1979).